We provide detailed responses below in black, with quotation marks showing the changes made in the manuscript and associated line numbers on the final (un-tracked) manuscript.

Author Response to Reviewer #2

This paper presents the results of a high number of model simulations performed to derive runoff from Greenland Ice Sheet as a function of black carbon deposition. The model is using state-of-the art snow model, which includes interactions of Light Absorbing Impurities (LAI) with solar radiation, as well as scavenging by meltwater. They also provide linear equations that relate the increase of total runoff to black carbon deposition. Their results could be used by climate models, which don't have a sophisticated snow model but would like to estimate total runoff from Greenland for a given black carbon deposition rate.

The paper is well written, their approach valid, and their results interesting. I have only few minor comments.

Minor comments: All the figures showing time series with one line per month would gain in clarity by reducing to one month per season.

As the reviewer suggested, we tried to make figures with seasonal curves. However, because the seasonal cycle differs among the quantities shown in the different figures, the seasonal plots become confusing. We provide here two seasonal plots for Figure 5 and 6 as examples, which we cannot see clear seasonal patterns for both wet and dry BC deposition fluxes. Thus, we decide not to change the figures in the manuscript.
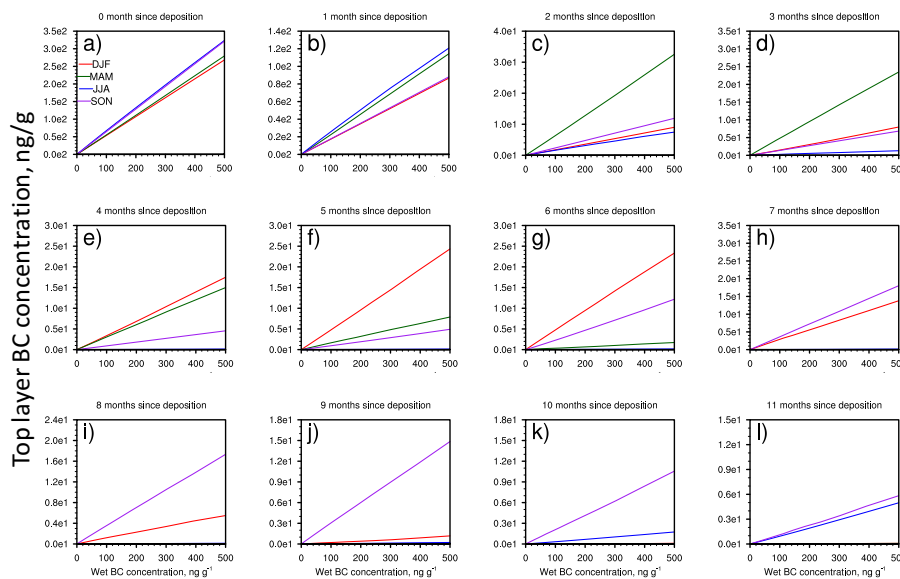

Figure R1. Hydrophilic BC concentration in the top snow layer vs. concentration of BC in precipitation shown at different times (0-11 months, panels a-l) since deposition. The top-snow layer concentrations are averaged over the Greenland region and over ten one-year simulations beginning in years 2006-2015. Different line colors represent different deposition seasons.
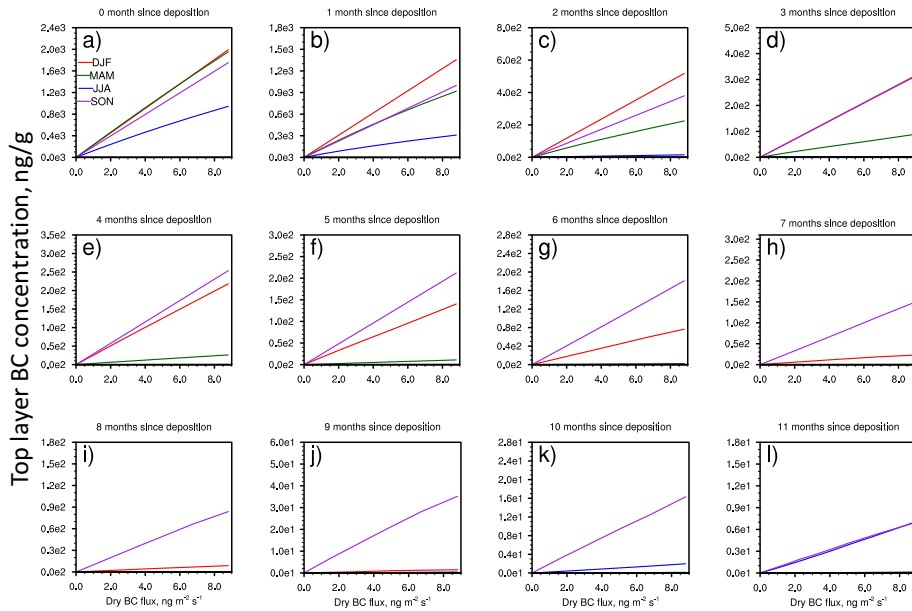
Figure R2. Same as Figure R1, but showing hydrophobic BC concentration in the top snow layer vs. BC dry deposition flux.

Are you assuming linearity of surface albedo change by black carbon deposition and metamorphism of snow grains? Should there not be another entry in the kernel for surface temperature?

We agree that surface temperature influences metamorphism of snow grains. However, as the reviewer also pointed out, the main difficulty of climate models is the lack of sophisticated snow model which relates total runoff with black carbon deposition. Therefore, we aimed to find out only the relationship between the amount of black carbon deposition and snow melt in our study. We didn't assume a linear relationship, but based on our simulations and calculations, we found linear regression could appropriately represent this relationship. Thus, we were able to provide linear equations relating the increase of total runoff to black carbon deposition.

It is unclear if the timestep of the snow model is one month, or sub-daily with the kernel data calculated as mean monthly values. If the timestep is monthly then the results for sub-daily timestep may have been quite different. At least an estimated error should be provided in such case.
Another needed precision is about spatial resolution. Line 98 we learned that CRUNCEP input data is 0.5 degree resolution. Is it the same for CLM and the kernel data?

We thank the reviewer for pointing out the confusion of temporal and spatial resolutions. Although the kernel data was calculated as monthly mean values, the timestep of the snow model implemented in our study was actually 0.5 hour. The resolution of CLM is 0.9° x 1.25°. And it is the same for the kernel data.

We add an explanation in Line 159 that "The timestep of CLM/SNICAR for our simulations is 0.5 hour, and the spatial resolution is 0.9° x 1.25°. The kernel product is calculated as monthly mean values with the same spatial resolution."

Line 141 "dry" should be "wet"

This was not a typo. We were trying to use the maximum wet BC deposition flux to calculate the maximum dry deposition flux, and then to implement this value to set up a set of dry BC fluxes with logarithmic spacing.

Line 177: "… as new snowfall dilutes the contaminated snow". Are you mixing layers and not superimposing them? LAI cannot move up in your model, right?

In CLM, snow layers can be combined and divided, as the maximum number of layers is fixed at 5, and both minimum and maximum thicknesses are prescribed for each layer. When layers are combined (e.g., because a layer thickness drops beneath the minimum threshold due to melt), both snow mass and BC mass are added together to establish the properties of the new layer. When the top layer exceeds the maximum thickness (2cm), e.g., due to new snowfall, the excess snow mass and a proportionate amount of BC are 'mixed down' into the layer beneath. We have specified these processes in Line 115, "Deposited particles are assumed to be instantly mixed and homogeneous within the surface snow layer", and "Particle masses are redistributed vertically in each time step proportionately with snow melt through the snow column, scaled by the species-specific melt scavenging efficiency, and snow layer combination and subdivision."

Lines 249-252: Is this due to an amplification effect by metamorphism of snow?

It could be. I added this hypothesis in Line 254 that "This could also be due to an amplification effect by metamorphism of snow in warmer years."

Line 262: "runoff… higher temperature" Is this increase of runoff by higher temperature due to darkening by black carbon or larger grain size?

That's a good point. We add the explanation in Line 265 that "The largest perturbation in summer could be caused by immediate melting due to darkening, as well as larger grain size in warmer environment."

Lines 279-280: "higher light absorptivity of hydrophilic BC" seems to contradict the values of single scattering albedo provided for black carbon in Table 3.5 of Oleson et al. (2013). The single scattering albedo of hydrophobic black carbon is lower than hydrophilic black carbon, indicative of stronger absorption by hydrophobic BC.

We agree that the single scatter albedo (SSA) is indeed lower for hydrophobic BC. However, the mass absorption cross section (MAC; product of the mass extinction cross section and co-SSA) is higher for hydrophilic BC. For absorption perturbations within a highly scattering medium like snow, MAC is the more relevant metric of absorptivity than SSA.

Line 281: "weakly-absorbing sulfate" Sulfate is purely scattering.

The assumed SSA value of sulfate is technically slightly less than 1.0, but we agree with the reviewer's point and have revised this reference to "non-absorbing sulfate" in Line 285.

1 Investigating the Impact of Aerosol Deposition on Snow

2 Melt over the Greenland Ice Sheet Using a Large-Ensemble

3 Kernel

4 Yang Li[1], Mark G. Flanner[1]

5 [1] Climate and Space Sciences and Engineering, University of Michigan, Ann Arbor, Michigan, USA

6

7 **Correspondence to:** Y. Li, yanglibj@umich.edu

8

9 **Abstract**

10 Accelerating surface melt on the Greenland Ice Sheet (GrIS) has led to a doubling of

11 Greenland's contribution to global sea level rise during recent decades. Black

12 carbon (BC), dust, and other light absorbing impurities (LAI) darken the surface and

13 enhance snow melt by boosting the absorption of solar energy. It is therefore

14 important for coupled aerosol-climate and ice sheet models to include snow

15 darkening effects from LAI, and yet most do not. In this study, we conduct several

16 thousand simulations with the Community Land Model (CLM) component of the

17 Community Earth System Model (CESM) to characterize changes in melt runoff due

18 to variations in the amount, timing, and nature (wet or dry) of BC deposition on the

19 GrIS. From this large matrix of simulations, we develop a kernel relating runoff to

20 the location, month, year (from 2006-2015), and magnitudes of BC concentration

21 within precipitation and dry deposition flux. BC deposition during June-August

22 causes the largest increase in annually-integrated runoff, but winter deposition

23   events also exert large (roughly half as great) runoff perturbations due to re-

24   exposure of impurities at the snow surface during summer melt. Current BC

25   deposition fluxes simulated with the atmosphere component of CESM induce a

26   climatological-mean increase in GrIS-wide runoff of ~8 Gt/yr, or +6.8% relative to a

27   paired simulation without BC deposition. We also provide linear equations that

28   relate the increase in total runoff to GrIS-wide wet and dry BC deposition fluxes. It

29   is our hope that the runoff kernel and simple equations provided here can be used

30   to extend the utility of state-of-the-art aerosol models.

1 Introduction

The Greenland Ice Sheet (GrIS) holds the equivalent of about 7 m of sea level rise (Kintisch, 2017). During recent decades, the accelerating decline of the GrIS has doubled Greenland's contribution to global sea level rise to about 0.74 mm per year (Shepherd et al., 2012; Rignot and Kanagaratnam, 2006; van den Broeke et al., 2009; Kintisch, 2017). Mass loss from the GrIS is predicted to raise sea level by more than 20 cm by 2100 (Rignot et al., 2011; Dumont et al., 2014), imposing tremendous effects on global society.

Ice loss from the GrIS is caused by many physical and biological factors, including: 1) increase of air temperature over the Arctic region, which accelerates surface melting; 2) declining surface albedo, which can be caused by a variety of effects including increased melt area, enhanced snow metamorphism, and accumulation of light-absorbing impurities (LAI) (Tedesco et al., 2016; Box et al., 2012; Dumont et al., 2014; Keegan et al., 2014; Shimada et al., 2016; Polashenski et al., 2015); and 3) calving of icebergs and submarine melting due to ice dynamics and changes of ocean temperature (Krabill et al., 2004; Zwally et al., 2002; Dumont et al., 2014). Since 2005, surface melting has likely contributed more to ice loss than iceberg calving (Kintisch, 2017). Sources of LAI include black carbon (BC), mineral dust, and algae and bacteria growing on the wet surface of the ice sheet, all of which darken the surface, boost the absorption of insolation and enhance snow melt.

BC is a major anthropogenic pollutant originating from fossil fuel combustion, open biomass burning, and biofuel use, and is a key LAI because its solar

3

53 absorptivity is extremely high (e.g., Bond et al., 2013). Previous climate modeling

54 studies simulate annual warming in the Arctic region with the inclusion of BC in

55 snow (Flanner et al., 2007; Flanner et al., 2009; Hansen and Nazarenko, 2004;

56 Hansen et al., 2005; Jacobson, 2004), and find BC/snow forcing induces a global

57 temperature response about three times greater than equal forcing from CO_2

58 (Flanner et al., 2007). BC influences snow coverage by warming the atmosphere,

59 reducing surface insolation through "dimming", and reducing snow reflectance

60 through darkening caused by BC deposition to snow surface. Globally, the darkening

61 effect within snow increases solar heating of snowpack, and exceeds the loss of

62 absorbed energy from dimming, causing a positive net surface forcing and

63 snowpack melting (Flanner et al., 2009). Melting snow also tends to retain BC

64 aerosols, which darken the surface more and increase absorption of insolation (e.g.,

65 Doherty et al., 2013). Therefore, it is important for coupled aerosol-climate and ice

66 sheet models to include BC darkening effects, and yet most do not.

67   Global BC emissions from fossil fuel and biofuel combustion have increased

68 dramatically during the industrial era. Since the early 20th century, BC emissions

69 also shifted spatially, decreasing in North American and Europe but increasing in

70 Asia (Bond et al., 2007; Bond et al., 2013). Both the spatial pattern of emissions and

71 the circulation features that are coincident with emissions can strongly effect the

72 amount of BC reaching the Arctic and depositing to the GrIS (Doherty et al., 2010;

73 Thomas et al., 2017; Jiao et al., 2014).

74   In this study, we develop a BC deposition-snow melt kernel using the

75 Community Earth System Model (CESM) to investigate changes in snow melt and

4

76 surface runoff due to variations in the amount and timing of aerosol deposition on

77 the GrIS. More than 5000 simulations are conducted with the Community Land

78 Model (CLM) component of CESM, driven with a large range of wet and dry BC

79 deposition fluxes to determine relationships between snow melt perturbation and

80 deposition amount occurring in different months. The final kernel product is

81 resolved by type of BC deposition (wet or dry), deposition amount, deposition

82 month, and deposition year ranging from 2006-2015. It is our hope that this kernel

83 will benefit regional and global aerosol modeling communities by allowing them to

84 estimate GrIS snow melt and surface runoff perturbations associated with different

85 aerosol deposition fluxes.

86 **2 Methods**

87 **2.1 Simulation design**

88   We use the Community Earth System Model (CESM) version 1.2.2, and run the

89 offline Community Land Model (CLM) (Oleson et al., 2013) version 4.5 with

90 prescribed wet or dry BC deposition in the snow sub-model to study the effects of

91 BC deposition on snow melt and runoff from Greenland. Our motivation for using

92 CLM in this offline configuration is that (1) it reduces noise associated with ocean

93 and atmosphere variability, enabling clearer identification of the runoff signal

94 caused by snow perturbations, and (2) the simulations are computationally cheap,

95 allowing us to explore a large parameter space. We drive the simulations using

96 meteorological forcing data from the Climatic Research Unit and National Centers

97 for Environmental Prediction (CRUNCEP) (Viovy, 2012) over the period 2006-2016.

5

98   CRUNCEP data cover the global land surface at a spatial resolution of a $0.5° \times 0.5°$,

99   and are provided with relatively low latency, allowing us to explore conditions over

100   the recent past. In CLM, the representation of terrestrial snow, including over ice

101   sheets, is based loosely on the SNTHERM model (Jordan, 1991) and is described in

102   detail by Oleson et al., 2013. Snow albedo and solar absorption within each snow

103   layer are simulated with the Snow, Ice, and Aerosol Radiative Model (SNICAR),

104   which accounts for solar zenith angle, albedo of the substrate underlying snow,

105   mass concentrations of LAI (black carbon, dust, organic carbon, and volcanic ash),

106   and ice effective grain size. In general, CLM/SNICAR represents five vertical snow

107   layers, and accounts for variations in LAI concentration due to dry and wet

108   deposition, particle flushing and retention with melt water, snow sublimation, and

109   layer combinations and divisions (Oleson et al., 2013). Dry BC deposition from the

110   atmosphere occurs through gravitational settling and turbulent mixing, primarily

111   transferring hydrophobic BC to the surface, while wet BC deposition occurs via

112   precipitation and only affects hydrophilic BC in the model. CLM maintains mass

113   burdens of both hydrophilic BC and hydrophobic BC within each snow layer, with

114   each species having unique optical properties and meltwater removal efficiencies.

115   Deposited particles are assumed to be instantly mixed and homogeneous within the

116   surface snow layer, which does not exceed 2 cm in thickness. The particles are

117   added after the computation of inter-layer water fluxes, thus preventing particles in

118   the top layer from being washed out immediately before radiative calculations.

119   Particle masses are redistributed vertically in each time step proportionately with

120   snow melt through the snow column, scaled by the species-specific melt scavenging

6

121 efficiency, and snow layer combination and subdivision. The masses carried out

122 with meltwater drainage through the bottom snow layer are permanently lost from

123 the snowpack, and are not maintained within the model (Oleson et al., 2013).

124   For each simulation used to generate the kernel relating melt runoff to BC

125 deposition, we prescribe uniform concentrations of BC within precipitation or

126 uniform dry deposition fluxes over the ice sheet for a period of one month, and

127 quantify perturbations to snow and melt runoff for one year or more following the

128 period of deposition. 23 unique BC concentrations in precipitation (e.g., snow) are

129 prescribed to provide wet BC flux in the CLM. We use a wide range of wet BC

130 concentrations (from 1 ng g^{-1} ~ 500 ng g^{-1}) with logarithmic spacing, aiming to

131 cover historically observed BC concentrations over the Greenland region (Figure 1)

132 and potential severe episodes associated (e.g.,) with extreme fire activity. For

133 example, measured values of BC in Greenland snow during 2012-2014, collected

134 from snow pits across a long transect, averaged 2.6 ng g^{-1} (Polashenski et al.,

135 2015). Peak values throughout the depth of the snow pits averaged 4 ng g^{-1} and 15

136 ng g^{-1} in 2012 and 2013, respectively, and the largest single measurement was 43 ng

137 g^{-1}. Ice core measurements from D4 dating back to 1788 show annual-mean

138 concentrations peaking in the early 20th century at ~12.5 ng g^{-1}, mean

139 concentrations of 2.3 ng g^{-1} during 1952-2002, and occasional monthly-mean peaks

140 exceeding 50 ng g^{-1} due to biomass burning events (McConnell et al., 2007).

141 Correspondingly, the maximum dry BC deposition flux is calculated as the product

142 of the maximum wet BC concentration (500 ng g^{-1}) and the mean monthly snowfall

143 (1.75×10^{-5} mm s^{-1}) over an 11-year (2006-2016) CESM simulation. We prescribe 24

144 unique dry BC fluxes (0.01 ng m^{-2} s^{-1}-8.80 ng m^{-2} s^{-1}) with logarithmic spacing in our

145 study (Figure 1).

146 With each prescribed BC deposition value, we perform 12 simulations with

147 specified BC deposition month from January to December in each deposition year.

148 Each simulation starts from January in the deposition year, and extends to one full

149 year after the deposition month in order to study the annually integrated BC effects.

150 We then repeat these simulations for ten years (2006-2015) to generate a

151 climatological product and explore the magnitude of interannual variability in melt

152 perturbations due, for example, to differences in precipitation and near-surface air

153 temperatures. In summary, we perform 2,760 simulations (23 wet BC

154 concentrations × 12 deposition months × 10 deposition years) to study the effects of

155 wet BC deposition, and 2,880 simulations (24 dry BC fluxes × 12 deposition months

156 × 10 deposition years) to study the effects of dry BC deposition. 120 simulations (12

157 deposition months × 10 deposition years) without BC deposition are also performed

158 as parallel control/base runs from which to derive the perturbations induced by BC

159 deposition. The timestep of CLM/SNICAR for our simulations is 0.5 hour, and the

160 spatial resolution is 0.9° x 1.25°. The kernel product is calculated as monthly mean

161 values with the same spatial resolution.

162 **2.2 Simulation length evaluation based on top-snow layer BC concentration**

163 To evaluate the importance of simulation length for the purposes outlined, we

164 focus on BC concentration in the top snow layer because properties of this layer

165 dominate the bulk solar radiative properties of the snowpack. In Figure 2, we

166 examine the mean distribution of BC concentration in the top snow layer over

8

167 Greenland after maximum wet and dry BC deposition fluxes occur in January and

168 June. These contours are averaged over ten years to show a climatological state.

169 Top-layer BC concentrations after wet BC deposition show higher values in the

170 center and south margin of Greenland (Figure 2a, b, e, f), which matches the general

171 precipitation pattern over the GrIS, with elevated precipitation amount in the center

172 and south of GrIS. Meanwhile, higher top-layer BC values occur over the north of

173 Greenland after dry BC deposition (Figure 2c, d, g, h), as lower precipitation in these

174 regions enhances the effect of dry deposition. Also, we find lower concentrations

175 induced by the maximum wet BC (Figure 2a, b, e, f) than by the maximum dry BC

176 deposition (Figure 2c, d, g, h). Top-layer BC concentration decreases rapidly only

177 one month after the deposition month for both winter and summer deposition (i.e.,

178 from January to February with January deposition in Figure 2a-d, and from June to

179 July with June deposition in Figure 2e-h), as new snowfall dilutes the contaminated

180 snow. The rapid decrease in BC concentration supports the notion that a one-year

181 simulation length should capture most of the time-integrated effect from a

182 deposition event. To verify this, we also perform two 11-year (2006-2016)

183 simulations with the maximum wet BC deposition occurring in April and October of

184 the first year, to evaluate the long-term variation of top-layer BC concentration. In

185 these long-term simulations, we find top-layer BC concentrations decrease rapidly

186 within a one-year period after both spring and fall depositions (Figure 3). We also

187 see, however, that residual BC reappears at the surface in subsequent summers

188 because of snow melting and associated accumulation of impurities at the top of the

189 snowpack (Doherty et al., 2013). In the model, this occurs because melt scavenging

9

190 ratios for both types of BC are less than 1, meaning that proportionately less BC

191 moves down vertically in the column than meltwater. As we will see, summer re-

192 appearance of impurities at the snow top has a non-negligible impact on the

193 annually-integrated runoff perturbation, but the peaks in subsequent years are less

194 than 1/20 of the BC concentrations in the deposition month, indicating that the one-

195 year simulation setup is reasonable to capture the major portion of the total BC

196 influences.

197 **3   Results and Discussion**

198   Deposited BC to snow causes a darkening effect and enhances snow melt and

199 Greenland runoff. Here, we first show variations of top-snow layer BC

200 concentrations, and then examine total GrIS runoff perturbation induced by BC

201 deposition.

202 **3.1   BC concentration in the top snow layer**

203   We investigate the climatological (i.e., averaged over ten simulations covering

204 2006-2015) 1-year evolution of top-snow layer BC concentration averaged over

205 Greenland for different deposition months. Figure 4 depicts the temporal evolution

206 of top-layer BC concentration for the maximum wet and dry BC fluxes from our

207 matrix of simulations. For all months of deposition, top-layer concentrations

208 decrease rapidly as fresh snow covers the contaminated surface. Top-snow layer

209 concentrations of dry-deposited BC generally decrease more slowly than those of

210 wet-deposited BC. One reason for this behavior during summer months is that dry-

211 deposited BC is assumed to be hydrophobic and have a lower meltwater scavenging

10

212 efficiency, reducing the rate at which it is carried away by melting water. We also

213 see, however, that some winter-deposited BC can persist in the top layer until, or

214 even re-appear during, the summer melt season, indicating that BC deposition in

215 non-melting seasons can also be important for GrIS melting. Re-exposure of

216 previously deposited BC occurs as overlying snow melts and flushes through the

217 snow, removing some but not all of the underlying impurities and eventually

218 exposing the dirty snow layer at the surface.

219   We also investigate how top-layer BC concentration varies with different BC

220 deposition values, and how this variation evolves over one year following

221 deposition (Figure 5 and Figure 6). For all deposition months, top-snow layer BC

222 concentration increases, as expected, with increasing BC deposition flux. The

223 relationship between top-layer BC concentration and BC deposition value is nearly

224 linear, although we find indications of saturation at later times with dry BC

225 deposition (e.g., as in Figure 6h-l). Figure 7 summarizes top-layer BC concentration

226 variation with deposition amount at different times (0-11 months since deposition)

227 averaged over all the deposition months. With this averaging, we find that top-layer

228 BC concentrations decrease monotonically from month 0 to month 11. Again, we

229 find slower decrease in the dry deposition simulations than in the wet deposition

230 simulations. With wet BC deposition, the rate of decrease slows down after 3-6

231 months, which could be due to the summer peaks resulting from snow melting and

232 BC integration (Figure 4).

233 **3.2   Temporal variation of GrIS total runoff**

234   We define total runoff in CLM as the summation of surface runoff, sub-surface

235   drainage and runoff from glacier surface. We first examine the seasonal and inter-

236   annual variation of GrIS total runoff, integrated over the entire GrIS, in the base run

237   without BC deposition (Figure 8). Total runoff shows clear summer peaks and some

238   inter-annual variation. Annual-integrated total runoff is ~120 Gt per year, with the

239   highest value of ~140 Gt in 2014 (Figure 8b). Compared with satellite gravity

240   measurements during 2005-2010 showing Greenland is losing mass at a rate of

241   ~229 Gt/yr (169-290 Gt/yr), of which 50-70% is lost through surface melt

242   (Vaughan et al., 2013), the simulated total runoff in the base run in our study is

243   within a reasonable range.

244   We then calculate perturbed total runoff due to BC deposition as the difference

245   in runoff between simulations with BC deposition and paired base simulations

246   without BC deposition. We select three wet BC deposition values and three dry BC

247   deposition values to illustrate the seasonal and inter-annual variations of perturbed

248   total runoff (Figure 9). We note that different scales are used in the panels of Figure

249   9, which shows that higher deposition causes more total runoff. We also find clear

250   inter-annual variations for different deposition amounts and months. The variations

251   of perturbed total runoff in Figure 9 follow the variation of total runoff in the base

252   run (Figure 8) in general, especially for the perturbed simulations with wet BC

253   depositions, indicating that BC deposition could have greater effect in warmer years,

254   when more of the ice sheet is near the melting temperature. This could also be due

255   to an amplification effect by metamorphism of snow in warmer years.

256   To remove the effect of yearly variation, we also investigate the climatological

257   (i.e., averaged over ten simulations spanning 2006-2015) 1-year evolution of total

12

258 runoff increase due to BC deposition starting from different deposition months.

259 Again, we examine total runoff increase induced by maximum wet and dry BC

260 depositions to understand general behavior associated with very large

261 perturbations, for which the signal is much larger than noise. As shown in Figure

262 10, we find two summer peaks of total runoff increase, with the second peak caused

263 by the re-exposure of BC during the summer after deposition. We also find total

264 runoff perturbation is the largest in July for all months of deposition, followed by

265 August. The largest perturbation in summer could be caused by immediate melting

266 due to darkening, as well as larger grain size in warmer environment.

3.3   GrIS total runoff variation with deposition amount

268   As represented by Figure 9, higher deposition amount causes larger total runoff

269 increase. Here, we examine total runoff perturbation caused by all deposition

270 amounts, and how total runoff distributes over Greenland. Figure 11 and Figure 12

271 show climatological mean (2006-2015) annually integrated total runoff increase

272 caused by June BC deposition via wet and dry processes, respectively. June

273 deposition is selected for these figures because of its high potential to impact

274 summer melt. Although BC is well distributed over the whole GrIS (Figure 2), total

275 runoff perturbations are largely confined to the low elevation margins with both

276 wet and dry BC deposition (Figure 11 and Figure 12), as these remain the only areas

277 warm enough in the model simulations for substantial melt to occur, which is

278 consistent with the Tedesco, 2007 study. We note that the spatial distribution of

279 model melt will be sensitive to surface air temperature and insolation, the latter of

280 which can vary substantially between re-analysis products. Runoff effects of dry BC

Deleted: , due to higher temperature in summer

282 deposition show similar patterns as impacts from BC in precipitation. We find that

283 small fluxes of BC via dry deposition are not as effective as similar deposition fluxes

284 of BC in precipitation, and we attribute this to the higher light absorptivity (and

285 hence radiative forcing per unit mass) of hydrophilic BC than of hydrophobic BC.

286 The former is assumed to be coated with non-absorbing sulfate and hence its mass

287 absorption cross-section is about 50% larger than that of uncoated hydrophobic BC

288 (Flanner et al., 2007).

289   Figure 13 summarizes the variation of total runoff perturbation versus

290 deposition amount for different deposition months. The maximum BC deposition

291 perturbs total runoff by up to ~20% (24 Gt) in the wet BC deposition simulations,

292 although we note that continent-wide fluxes of this magnitude (500 ng g^{-1} in

293 precipitation) are much larger than ever observed on Greenland. With a modest

294 deposition concentration (e.g., 5 ng/g), the runoff perturbation is ~0.4% (~0.5 Gt).

295 Different deposition months cause annually integrated total runoff perturbation to

296 vary by 40-60% (12 Gt/yr in the maximum BC deposition case). Also, we find BC

297 deposition in June and July induces the largest annually integrated total runoff

298 increase. To further verify the most influential deposition month, we select five wet

299 BC and five dry BC deposition values, and plot total runoff increase versus

300 deposition month, shown in Figure 14. Figure 14a shows annual integrated total

301 runoff from the base run, starting from different months, serving as a reference for

302 the perturbations shown in Figure 14b-f. For different deposition amounts from low

303 to high (Figure 14b-f), BC deposition in summer (i.e., June, July and August) causes

304 the highest annual total runoff increase. With higher deposition (Figure 14e-f), June

Deleted: weakly

306   deposition generates the largest annual total runoff for both dry and wet BC

307   deposition, whereas with lower deposition amounts the month of maximum impact

308   can be June or July. As noted earlier, however, deposition during non-summer

309   months also causes substantial melt and runoff perturbations, owing to the melt-

310   induced re-surfacing of impurities during summer in the ablation zone.

311   **4   Evaluation and application of the kernel product**

312   We turn now to evaluating the kernel product and advising a straightforward

313   way in which it can be applied to realistic aerosol deposition fluxes. We perform ten

314   one-year CLM simulations with spatially and temporally-varying wet or dry BC

315   deposition fluxes occurring in randomly selected years and months, and we evaluate

316   the accuracy of the kernel product using total GrIS BC deposition amount and total

317   runoff from these new simulations (the "evaluating simulations"), compared with

318   total runoff from the kernel for equivalent deposition fluxes. The evaluating

319   simulations use prescribed wet and dry BC deposition fields that were generated

320   from a global aerosol run with CAM (Lamarque et al., 2010). In different evaluating

321   simulations, the prescribed BC deposition fields are multiplied by factors ranging

322   from 2-50 for wet BC deposition and 2000-20000 for dry BC deposition to provide

323   different BC deposition amounts within the range of wet or dry deposition in the

324   kernel. High scaling factors are applied to dry/hydrophobic BC deposition

325   simulations because the prescribed dry BC deposition from CAM is very low and

326   within the noise regime. We also perform two ten-year (2006-2015) evaluating

327   simulations with both CAM prescribed wet and dry BC deposition fluxes turned on

328   throughout the whole simulations, to examine short-term, long-term and

329   climatological one-year integrated total runoff effects. BC deposition fluxes in one of

330   the ten-year evaluating simulations are multiplied by a factor of 5 to provide a high

331   deposition event and are left at unperturbed (i.e., realistic) values in the other

332   simulation. Also, different deposition years and months indicate different BC

333   distributions. Therefore, the evaluating simulations provide a variety of scenarios

334   with distinct BC deposition amounts and distributions to evaluate performance of

335   the kernel.

336   Figure 15 shows maximum, mean and minimum one-year integrated total

337   runoff increase versus BC deposition amount from the kernel product, with results

338   from the evaluating simulations overlaid on the kernel lines. With varying BC

339   deposition amount and distribution, including with combined wet and dry BC

340   deposition fluxes, results from the evaluating simulations are mostly within the total

341   runoff ranges of our kernel product for both wet and dry BC deposition. In the

342   evaluating simulations with combined wet and dry BC depositions, hydrophobic BC

343   fluxes are very low (<1/100 of wet BC fluxes), therefore, we treat all BC deposition

344   as wet/hydrophilic BC, and overlay the results on the wet deposition curves. We

345   note CAM simulated BC deposition from the 1 time evaluating run is comparable

346   with measured values of BC in Greenland snow and ice core measurements

347   (Polashenski et al., 2015; McConnell et al., 2007). The increases of one-year

348   integrated total runoff from the ten-year evaluating simulations with realistic

349   deposition exhibit wide ranges, for example, with a minimum of ~4 Gt in the first

350   deposition year (2006) to a maximum of ~10 Gt, and with a minimum of ~14 Gt in

351 the first year to a maximum of ~40 Gt in the simulation with 5 times BC fluxes. The

352 climatological (i.e., averaged over 10 years) total runoff perturbations (~8 Gt/yr and

353 ~30 Gt/yr in the default and 5 times simulations, respectively) caused by prescribed

354 combined wet and dry BC deposition are about double the first-year total runoff

355 integrations, which is due to continuous month by month depositions in the ten-

356 year evaluating simulations and the long-term effects of the reappearance of

357 residual BC at the surface as described in section 2.2.

358   Because the mean and maximum kernel curves in Figure 15 provide estimates

359 of BC induced total runoff within a reasonable range, we parameterize these curves

360 to provide a simple application of our kernel product. GrIS-wide melt perturbations

361 are relatively linear with BC deposition amount, with linear fits to the mean kernel

362 curves for wet and dry BC deposition fluxes of, respectively:

363   ΔTOTALRUNOFF = 4.498e5 * ΔwetBC,   (1)

364   ΔTOTALRUNOFF = 3.062e5 * ΔdryBC,   (2)

365 and with linear fits to the maximum kernel curves of:

366   ΔTOTALRUNOFF_MAX = 9.322e5 * ΔwetBC,   (3)

367   ΔTOTALRUNOFF_MAX = 6.348e5 * ΔdryBC,   (4)

368 where ΔTOTALRUNOFF is the mean increase in one-year integrated total runoff (kg

369 yr^{-1}), ΔTOTALRUNOFF_MAX is the maximum increase in one-year integrated total

370 runoff (kg yr^{-1}), and ΔwetBC and ΔdryBC are total wet and dry BC deposition fluxes

371 to the GrIS (kg yr^{-1}). Unique relationships for wet and dry deposition arise, again,

372 because of differences in optical properties and melt-induced removal efficiencies of

373 hydrophilic and hydrophobic BC. Linearity in the relationship between runoff and

17

374 BC deposition is encouraging because we have neglected coincident darkening from

375 other types of LAI (e.g., dust, algae). In environments where darkening from other

376 LAI is not too great, the runoff–BC relationships derived here should be valid,

377 though we acknowledge that the incremental effect of BC will be lower in snow that

378 is heavily laden with other impurities.

379 The bulk relationships shown above represent the simplest application of our

380 kernel product, allowing a rough estimation of runoff perturbation caused by

381 Greenland-wide wet and dry BC deposition fluxes. Based on the evaluations in

382 Figure 15, the mean curves (i.e., equations (1) and (2)) from the kernel product tend

383 to provide a conservative estimate of total runoff, whereas the maximum curves

384 (i.e., equations (3) and (4)) represent a more realistic approximation of total runoff

385 induced by BC deposition that occurs continuously and with varying spatial

386 distribution. Ideally, gridcell-by-gridcell fluxes should be matched to the kernel to

387 account for spatial differences in melt associated with elevation and other

388 conditions (Figure 11 and Figure 12), but at the low end of deposition flux we see

389 considerable noise at the individual pixel and deposition month level, especially for

390 wet deposition fluxes that can be subject to anomalies associated with low

391 precipitation amounts in a given month. To ameliorate this, for typical present-day

392 deposition fluxes we recommend matching month-specific, but spatially-integrated

393 deposition fluxes or concentrations with the associated Greenland-wide kernel

394 values.

395 Finally, although this product only includes BC, we suggest that it could be

396 extended to include other LAI species through a simple scaling that accounts for the

397 ratio of mass-specific absorption between the species of interest and the BC

398 explored here. Rationale for this is that radiative forcing and melt perturbation will

399 scale roughly linearly with absorptivity, at least for relatively low and moderate

400 burdens of LAI. The mass-specific visible band absorption cross-sections assumed

401 in our study for hydrophilic (via wet deposition) and hydrophobic (via dry

402 deposition) BC are 7.5 and 11.3 $m^2\,g^{-1}$, respectively. The only other species-specific

403 property affecting results from this study is the meltwater scavenging coefficient,

404 which is assumed to be 0.2 for hydrophilic BC and 0.03 for hydrophobic BC (Flanner

405 et al., 2007). Given relatively large uncertainty in this parameter (Doherty et al.,

406 2013; Qian et al., 2014), we suggest applying the hydrophilic (wet deposition)

407 kernel to all hydrophilic species and the hydrophobic (dry deposition) kernel to all

408 hydrophobic species, along with appropriate scaling of optical properties.

409 **5   Conclusions**

410   In this study, ~6,000 simulations are performed to investigate annually

411 integrated runoff perturbation from BC deposition on snow. The simulation matrix

412 includes variations in deposition flux, deposition month and year, and nature of the

413 deposition (wet or dry). From this matrix we produce a large-ensemble kernel that

414 relates BC deposition fluxes to GrIS runoff perturbations.

415   In the month after deposition, top-snow layer BC concentration decreases

416 rapidly due to fresh snow coverage, but then increases somewhat in the ablation

417 zone during the following summer due to melt-induced re-exposure of the

418 contaminated snow. Accordingly, the total runoff increase induced by BC deposition

419   is substantial for both summer and winter deposition, though with peak impacts

420   associated with June and July deposition. Impacts from winter deposition suggest

421   that winter emissions, associated for example with biomass heating use, should not

422   be neglected as potential contributors to increased summer melt. Also, we find most

423   of the runoff increase occurs along the margins, and especially on the southern

424   margin of Greenland, with little sign of melting in the center of the GrIS where it is

425   rarely warm enough. Inter-annual variations in total runoff in the base and BC

426   perturbed simulations indicate that BC deposition can generate more impact in

427   warmer years, when more of the ice surface is near the melting temperature.

428   In summary, higher BC deposition amount leads to higher total runoff. We do

429   not find a clear sign of runoff saturation caused by high BC deposition values in our

430   study. Model-generated deposition fluxes associated with realistic BC emissions

431   induce a climatological-mean (2006-2015) GrIS-wide runoff increase of 8 Gt/yr

432   (+6.8% perturbation), which corresponds to 0.022 mm/year of global sea level rise.

433   We also suggest simple, linear equations that crudely relate GrIS-wide wet and dry

434   BC deposition fluxes to annually-integrated runoff perturbation, and provide links

435   to the full spatially-varying kernel dataset so that users can derive more accurate

436   estimates of melt perturbation (e.g., resolved by seasonal timing) from deposition

437   fluxes. We also suggest that the kernel results can be applied to other LAI species

438   via simple scaling of the mass absorption cross-section. Our hope is that these data

439   will extend the utility of state-of-the-art aerosol models.

440

21

References

Bond, T. C., Bhardwaj, E., Dong, R., Jogani, R., Jung, S., Roden, C., Streets, D. G., and
Trautmann, N. M.: Historical emissions of black and organic carbon aerosol from
energy-related combustion, 1850–2000, Global Biogeochemical Cycles, 21, n/a-
n/a, 10.1029/2006GB002840, 2007.
Bond, T. C., Doherty, S. J., Fahey, D. W., Forster, P. M., Berntsen, T., DeAngelo, B. J.,
Flanner, M. G., Ghan, S., Kärcher, B., Koch, D., Kinne, S., Kondo, Y., Quinn, P. K.,
Sarofim, M. C., Schultz, M. G., Schulz, M., Venkataraman, C., Zhang, H., Zhang, S.,
Bellouin, N., Guttikunda, S. K., Hopke, P. K., Jacobson, M. Z., Kaiser, J. W., Klimont,
Z., Lohmann, U., Schwarz, J. P., Shindell, D., Storelvmo, T., Warren, S. G., and
Zender, C. S.: Bounding the role of black carbon in the climate system: A scientific
assessment, Journal of Geophysical Research: Atmospheres, 118, 5380-5552,
10.1002/jgrd.50171, 2013.
Box, J., Fettweis, X., Stroeve, J., Tedesco, M., Hall, D., and Steffen, K.: Greenland ice
sheet albedo feedback: thermodynamics and atmospheric drivers, The
Cryosphere, 6, 821-839, 2012.
Doherty, S., Warren, S., Grenfell, T., Clarke, A., and Brandt, R.: Light-absorbing
impurities in Arctic snow, Atmospheric Chemistry and Physics, 10, 11647-11680,
2010.
Doherty, S. J., Grenfell, T. C., Forsström, S., Hegg, D. L., Brandt, R. E., and Warren, S. G.:
Observed vertical redistribution of black carbon and other insoluble light‐
absorbing particles in melting snow, Journal of Geophysical Research:
Atmospheres, 118, 5553-5569, 2013.
Dumont, M., Brun, E., Picard, G., Michou, M., Libois, Q., Petit, J. R., Geyer, M., Morin, S.,
and Josse, B.: Contribution of light-absorbing impurities in snow to Greenland's
darkening since 2009, Nature Geoscience, 7, 509, 10.1038/ngeo2180
https://www.nature.com/articles/ngeo2180#supplementary-information, 2014.
Flanner, M. G., Zender, C. S., Randerson, J. T., and Rasch, P. J.: Present-day climate
forcing and response from black carbon in snow, Journal of Geophysical
Research: Atmospheres, 112, n/a-n/a, 10.1029/2006JD008003, 2007.
Flanner, M. G., Zender, C. S., Hess, P. G., Mahowald, N. M., Painter, T. H., Ramanathan,
V., and Rasch, P.: Springtime warming and reduced snow cover from
carbonaceous particles, Atmospheric Chemistry and Physics, 9, 2481-2497, 2009.
Hansen, J., and Nazarenko, L.: Soot climate forcing via snow and ice albedos,
Proceedings of the National Academy of Sciences of the United States of America,
101, 423-428, 2004.
Hansen, J. e., Sato, M., Ruedy, R., Nazarenko, L., Lacis, A., Schmidt, G., Russell, G.,
Aleinov, I., Bauer, M., and Bauer, S.: Efficacy of climate forcings, Journal of
Geophysical Research: Atmospheres, 110, 2005.

487 Jacobson, M. Z.: Climate response of fossil fuel and biofuel soot, accounting for soot's
488   feedback to snow and sea ice albedo and emissivity, Journal of Geophysical
489   Research: Atmospheres, 109, 2004.
490 Jiao, C., Flanner, M., Balkanski, Y., Bauer, S., Bellouin, N., Berntsen, T., Bian, H.,
491   Carslaw, K., Chin, M., and De Luca, N.: An AeroCom assessment of black carbon in
492   Arctic snow and sea ice, Atmospheric Chemistry and Physics, 14, 2399-2417,
493   2014.
494 Jordan, R.: A one-dimensional temperature model for a snow cover: Technical
495   documentation for SNTHERM. 89, COLD REGIONS RESEARCH AND ENGINEERING
496   LAB HANOVER NH, 1991.
497 Keegan, K. M., Albert, M. R., McConnell, J. R., and Baker, I.: Climate change and forest
498   fires synergistically drive widespread melt events of the Greenland Ice Sheet,
499   Proceedings of the National Academy of Sciences, 111, 7964-7967, 2014.
500 Kintisch, E.: Meltdown, in, American Association for the Advancement of Science,
501   2017.
502 Krabill, W., Hanna, E., Huybrechts, P., Abdalati, W., Cappelen, J., Csatho, B., Frederick,
503   E., Manizade, S., Martin, C., and Sonntag, J.: Greenland ice sheet: increased coastal
504   thinning, Geophysical Research Letters, 31, 2004.
505 Lamarque, J.-F., Bond, T. C., Eyring, V., Granier, C., Heil, A., Klimont, Z., Lee, D.,
506   Liousse, C., Mieville, A., and Owen, B.: Historical (1850–2000) gridded
507   anthropogenic and biomass burning emissions of reactive gases and aerosols:
508   methodology and application, Atmospheric Chemistry and Physics, 10, 7017-
509   7039, 2010.
510 McConnell, J. R., Edwards, R., Kok, G. L., Flanner, M. G., Zender, C. S., Saltzman, E. S.,
511   Banta, J. R., Pasteris, D. R., Carter, M. M., and Kahl, J. D.: 20th-century industrial
512   black carbon emissions altered arctic climate forcing, Science, 317, 1381-1384,
513   2007.
514 Oleson, K., Lawrence, M., Bonan, B., Drewniak, B., Huang, M., Koven, D., Levis, S., Li, F.,
515   Riley, J., and Subin, M.: Technical description of version 4.5 of the Community
516   Land Model (CLM), 2013.
517 Polashenski, C. M., Dibb, J. E., Flanner, M. G., Chen, J. Y., Courville, Z. R., Lai, A. M.,
518   Schauer, J. J., Shafer, M. M., and Bergin, M.: Neither dust nor black carbon causing
519   apparent albedo decline in Greenland's dry snow zone: Implications for MODIS
520   C5 surface reflectance, Geophysical Research Letters, 42, 9319-9327, 2015.
521 Qian, Y., Wang, H., Zhang, R., Flanner, M. G., and Rasch, P. J.: A sensitivity study on
522   modeling black carbon in snow and its radiative forcing over the Arctic and
523   Northern China, Environmental Research Letters, 9, 064001, 2014.
524 Rignot, E., and Kanagaratnam, P.: Changes in the velocity structure of the Greenland
525   Ice Sheet, Science, 311, 986-990, 2006.
526 Rignot, E., Velicogna, I., van den Broeke, M. R., Monaghan, A., and Lenaerts, J. T.:
527   Acceleration of the contribution of the Greenland and Antarctic ice sheets to sea
528   level rise, Geophysical Research Letters, 38, 2011.
529 Shepherd, A., Ivins, E. R., Geruo, A., Barletta, V. R., Bentley, M. J., Bettadpur, S., Briggs,
530   K. H., Bromwich, D. H., Forsberg, R., and Galin, N.: A reconciled estimate of ice-
531   sheet mass balance, Science, 338, 1183-1189, 2012.

532 Shimada, R., Takeuchi, N., and Aoki, T.: Inter-annual and geographical variations in
533   the extent of bare ice and dark ice on the Greenland ice sheet derived from MODIS
534   satellite images, Frontiers in Earth Science, 4, 43, 2016.
535 Tedesco, M.: Snowmelt detection over the Greenland ice sheet from SSM/I
536   brightness temperature daily variations, Geophysical Research Letters, 34, 2007.
537 Tedesco, M., Doherty, S., Fettweis, X., Alexander, P., Jeyaratnam, J., and Stroeve, J.:
538   The darkening of the Greenland ice sheet: trends, drivers, and projections (1981–
539   2100), Cryosphere (The), 10, 477-496, 2016.
540 Thomas, J. L., Polashenski, C. M., Soja, A. J., Marelle, L., Casey, K., Choi, H. D., Raut, J. C.,
541   Wiedinmyer, C., Emmons, L. K., and Fast, J.: Quantifying black carbon deposition
542   over the Greenland ice sheet from forest fires in Canada, Geophysical Research
543   Letters, 2017.
544 van den Broeke, M., Bamber, J., Ettema, J., Rignot, E., Schrama, E., van de Berg, W. J.,
545   van Meijgaard, E., Velicogna, I., and Wouters, B.: Partitioning recent Greenland
546   mass loss, science, 326, 984-986, 2009.
547 Vaughan, D. G., Comiso, J. C., Allison, I., Carrasco, J., Kaser, G., Kwok, R., Mote, P.,
548   Murray, T., Paul, F., and Ren, J.: Observations: cryosphere, Climate change, 2103,
549   317-382, 2013.
550 Viovy, N.: CRU-NCEP Version 4, available at:
551   http://dods.extra.cea.fr/data/p529viov/cruncep/V4_1901_2012/ last access:
552   August 2012.
553 Zwally, H. J., Abdalati, W., Herring, T., Larson, K., Saba, J., and Steffen, K.: Surface
554   melt-induced acceleration of Greenland ice-sheet flow, Science, 297, 218-222,
555   2002.
556

Figure Captions
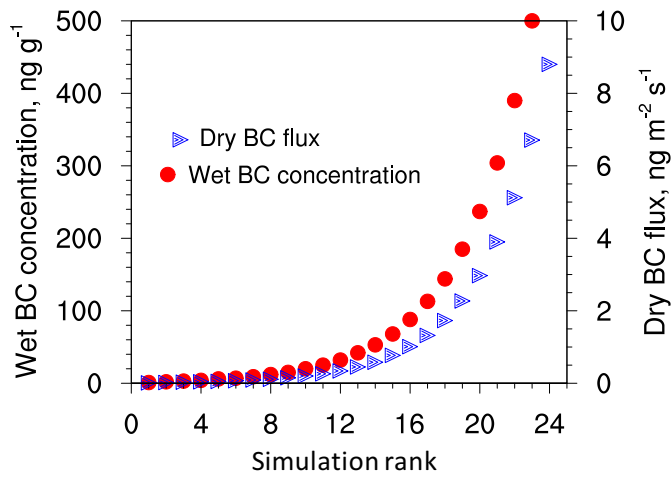
Figure 1. Prescribed values of BC concentrations in precipitation (red) and dry

deposition fluxes (blue) applied in the CESM modeling studies. Spacing between

values is logarithmic.
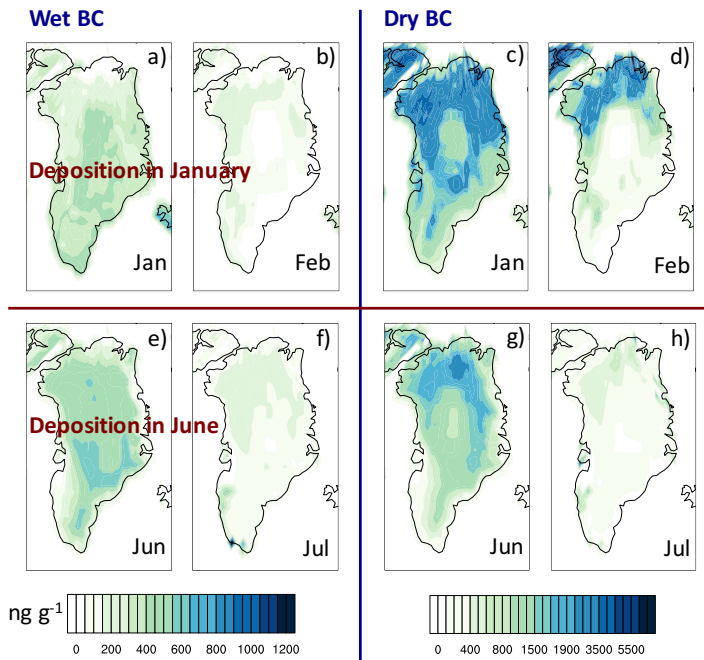
Figure 2. Ten-year (2006-2015) averaged hydrophilic BC concentration associated with wet deposition (a, b, e, f) and hydrophobic BC concentration associated with dry deposition (c, d, g, h) in the top snow layer. The contour maps show concentrations caused by January deposition (a-d) and June deposition (e-h), associated with the maximum wet and dry deposition scenarios depicted in Figure 1.

572
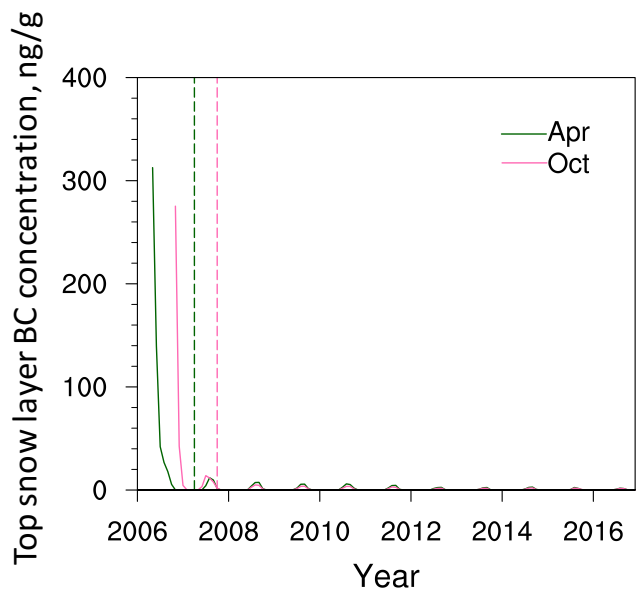
Figure 3. Temporal evolution of hydrophilic BC concentration in the top snow layer

averaged over the Greenland region from two 11-year (2006-2016) simulations

with wet BC deposition occurring in April and October of the first year. The BC

concentration in precipitation is the maximum value shown in Figure 1. Dashed

lines represent the ends of one year since different deposition months.

578

579
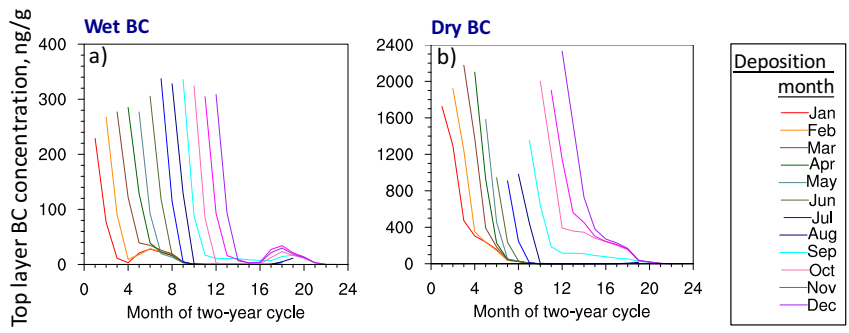
Figure 4. Temporal evolution of hydrophilic BC concentration (a) and hydrophobic

BC concentration (b) in the top snow layer averaged over the Greenland region from

the simulations with the maximum wet and dry BC deposition, respectively. Each

line starts from the BC deposition month, extends one year, and represents the

mean time series from 10 simulations that start in each year from 2006-2015.

585

28

586
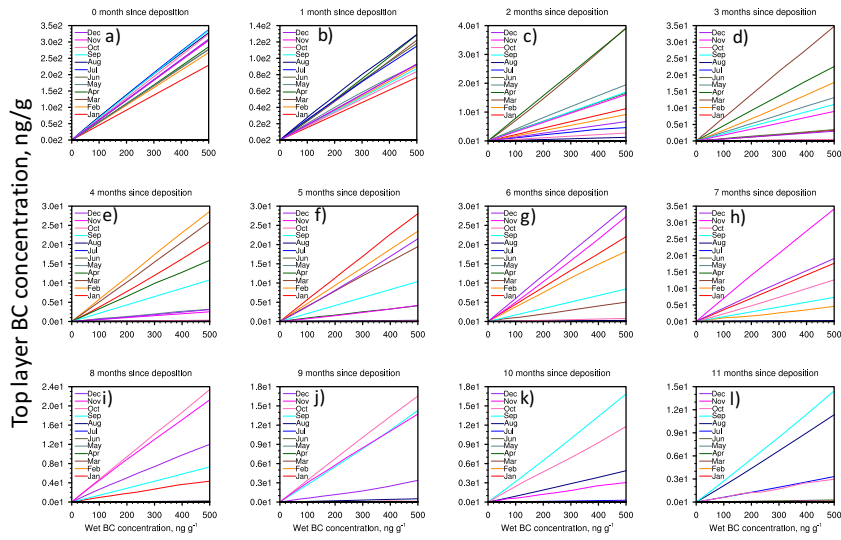
Figure 5. Hydrophilic BC concentration in the top snow layer vs. concentration of

BC in precipitation shown at different times (0-11 months, panels a-l) since

deposition. The top-snow layer concentrations are averaged over the Greenland

region and over ten one-year simulations beginning in years 2006-2015. Different

line colors represent different deposition months.

587

588

589

590

591

592

593
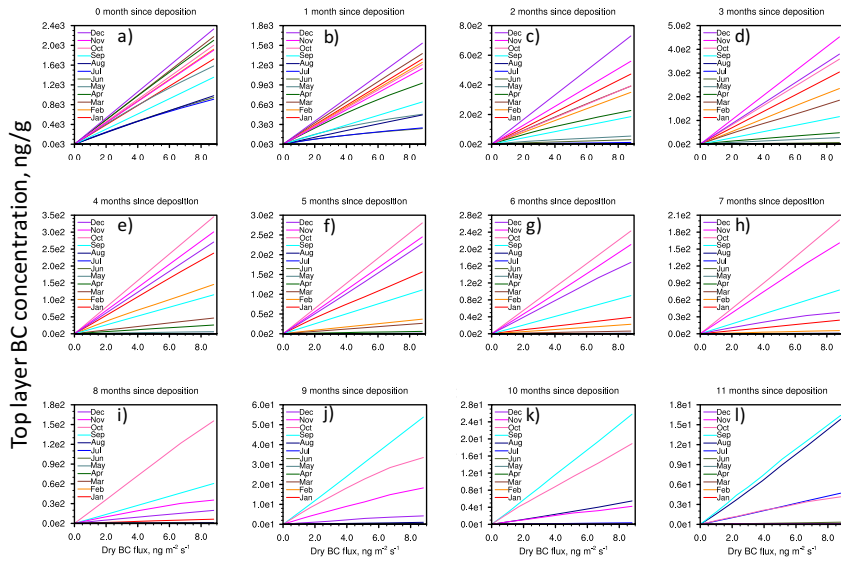
Figure 6. Same as Figure 5, but showing hydrophobic BC concentration in the top

595   snow layer vs. BC dry deposition flux.

596

597

598

599

600
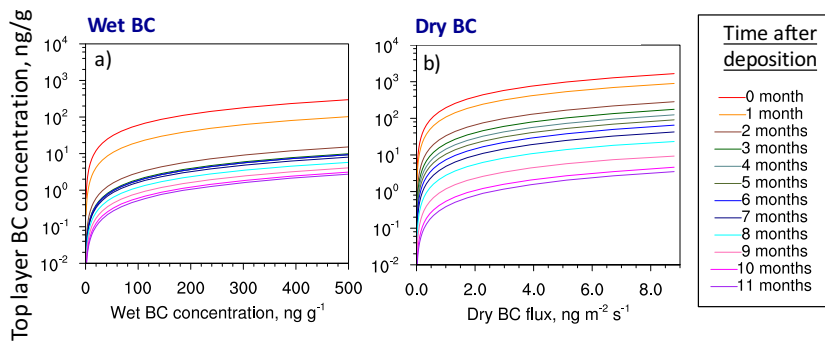
Figure 7. Hydrophilic BC concentration in the top snow layer vs. concentration of BC in precipitation (a), and hydrophobic BC concentration in the top snow layer vs. BC dry deposition flux (b) shown at different times (0-11 months) since deposition. The top-snow layer concentrations are averaged over the Greenland region, over all the deposition months and over ten one-year simulations beginning in years 2006-2015.
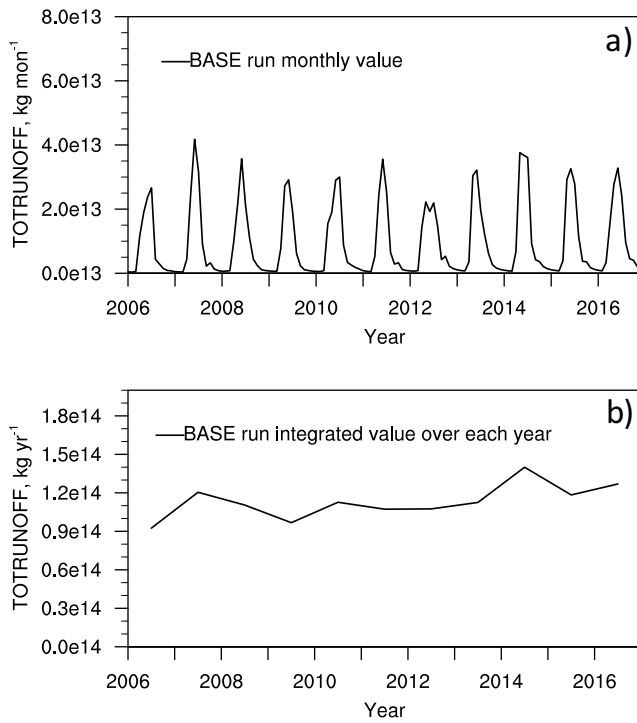
609

610 **Figure 8.** Monthly (a) and annually integrated (b) timeseries of total runoff from

611 Greenland in the Base run without BC deposition.

612

613
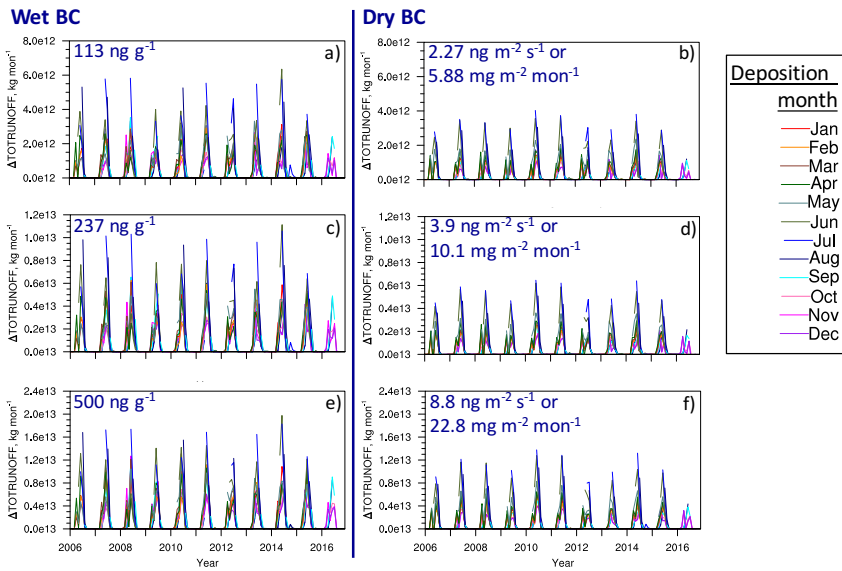
Figure 9. Monthly timeseries of the increase in total Greenland runoff resulting

from BC deposition. Values of BC concentrations in precipitation (a, c, e) and dry

deposition fluxes (b, d, f) are shown in each plot. Each line starts from the BC

deposition month and extends one year. Different line colors represent different

deposition months.

619

620
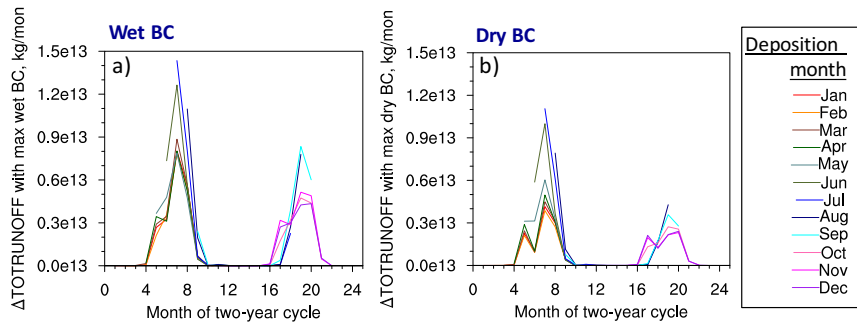
Figure 10. Temporal evolution of ten-year (2006-2015) averaged total runoff

increase resulting from BC deposition, summed over the entire Greenland region

from the simulations with the maximum wet (a) and dry (b) BC deposition. Each line

starts from the BC deposition month and extends one year.

625

10-year average of 12-month integrated ΔTOTRUNOFF since deposition in Jun

626
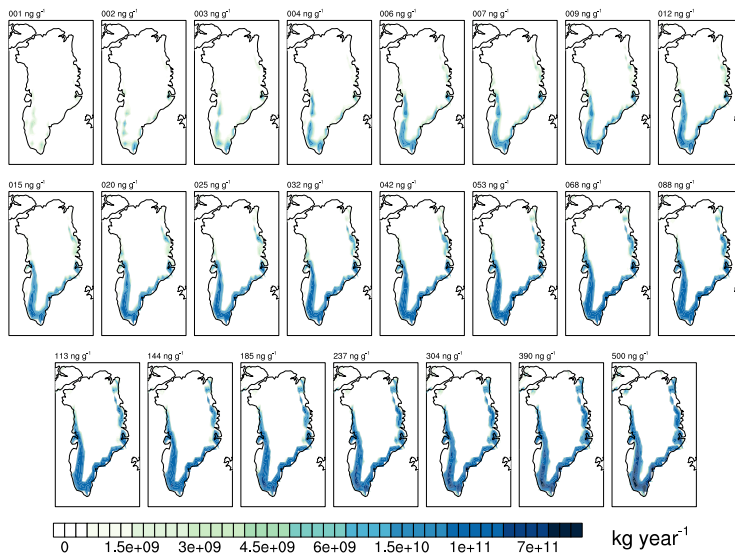
Figure 11. Ten-year average of annually-integrated total runoff increase resulting

from different concentrations of BC in precipitation, deposited only during June.

The average is over ten one-year simulations starting in each year from 2006-2015.

630

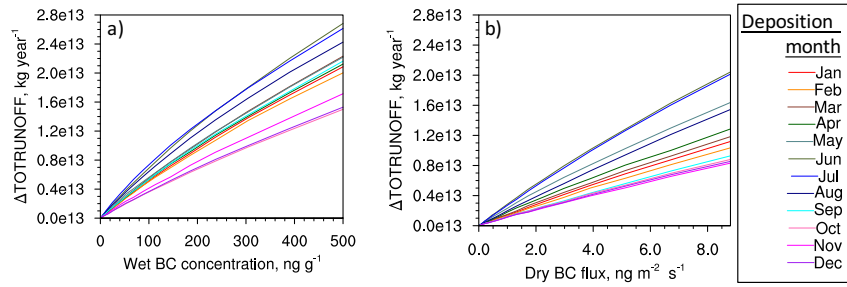10-year average of 12-month integrated ΔTOTRUNOFF since deposition in Jun
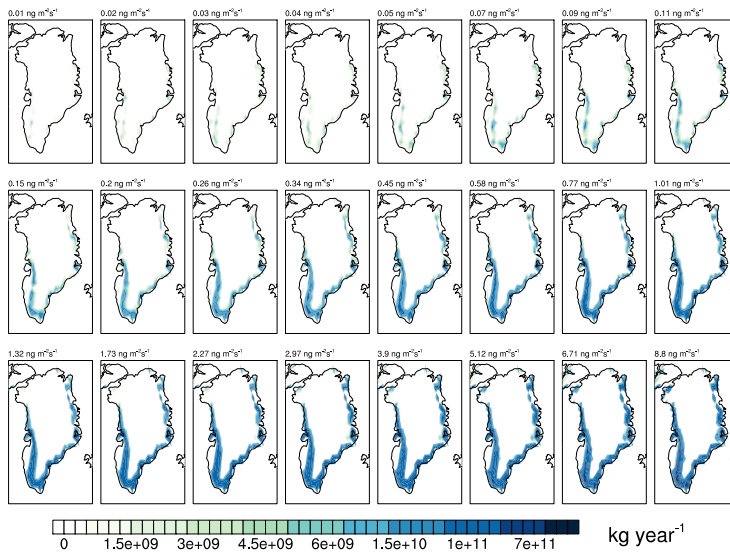
631

632   **Figure 12.** Same as Figure 11, but resulting from different dry deposition fluxes of

633   BC in June.

634

635

636

637

Figure 13. Increase in total Greenland runoff resulting from BC deposition

integrated over one year starting from the month of BC deposition vs. concentration

of BC in precipitation (a) and vs. BC dry deposition flux (b). The runoff values are

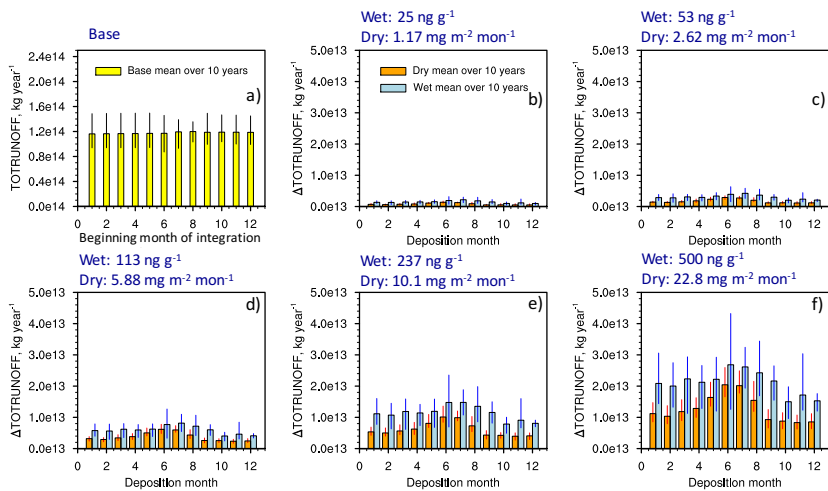summed over the Greenland region and averaged over ten one-year simulations

beginning in years 2006-2015. Different line colors represent different deposition

months.

644

645

646

Figure 14. Total runoff in the Base run without BC deposition (a) and the increase

in total Greenland runoff resulting from BC deposition (b-f), integrated over one

year starting from the month of BC deposition. The bars show mean values and the

whiskers depict the full range of values over all ten simulations that each start in a

different year from 2005-2016. Values of BC concentrations in precipitation and dry

deposition fluxes are shown in the title of each plot (b-f).

653

654
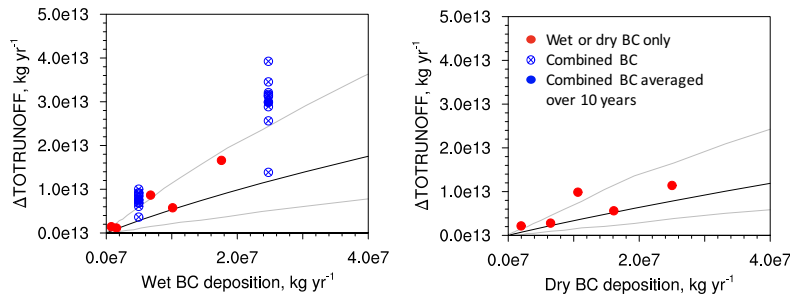
Figure 15. Increase in total Greenland runoff resulting from BC deposition

integrated over one year starting from the month of BC deposition vs. total wet (a)

and dry (b) BC deposition mass flux over the entire GrIS. The runoff values are

summed over the Greenland region and averaged over all deposition years and

deposition months. Black lines show mean total runoff values, and grey lines show

maximum and minimum values from the entire matrix of simulations. Red dots

represent explicitly-simulated total runoff from the evaluating simulations with

prescribed spatially and temporally-varying wet or dry BC deposition fluxes in

randomly selected months and years. Blue hollow circles represent simulated total

runoff from the evaluating simulations with prescribed combined BC deposition

fluxes integrated over each year of the ten-year simulations. Blue dots show

averages of the hollow circles.

667